ISSN 0016-7029, Geochemistry International, 2007, Vol. 45, No. 2, pp. 131–151. © Pleiades Publishing, Ltd., 2007.
Original Russian Text © Ya.V. Bychkova, E.V. Koptev-Dvornikov, N.N. Kononkova, E.E. Kameneva, 2007, published in Geokhimiya, 2007, No. 2, pp. 159–179.

Composition of Rock-Forming Minerals in the Kivakka Layered Massif, Northern Karelia, and Systematic Variations in the Chemistries of Minerals in the Rhythmic Layering Subzone

Ya. V. Bychkova[a], E. V. Koptev-Dvornikov[a], N. N. Kononkova[b], and E. E. Kameneva[a]

[a] *Division of Geology, Moscow State University, Vorob'evy gory, Moscow, 119992 Russia*
e-mail: yanab@geol.msu.ru

[b] *Vernadsky Institute of Geochemistry and Analytical Chemistry, Russian Academy of Sciences, ul. Kosygina 19, Moscow, 119991 Russia*

Received July 7, 2005

Abstract—Data obtained on the compositions of rock-forming minerals from the Kivakka layered intrusion indicate that the #Fe of olivine increases up the vertical section of the intrusion, and the #Mg of the pyroxenes and the anorthite contents of the plagioclase simultaneously decrease, which reflects the fractionation of the parental melt. Emphasis is placed onto the compositional variability of minerals in the layered unit. A method is developed for the reliable calculation of the composition of pyroxenes before their exsolution (separately for ortho- and clinopyroxene). The composition of minerals in the zone of intercalating melano-, meso-, and leucocratic norites remains practically unchanged, which is generally consistent with the results of mathematical simulations: compositional variations of the bronzite (#Mg) and plagioclase (*An* content) during the crystallization of the bronzite–plagioclase cotectic were no greater than 5 mol %. The variations in the concentrations of trace elements in the cumulus and intercumulus clinopyroxene occurred to be the most informative. It was determined that the Cr concentration in the cumulus augite is statistically significantly lower than that in the intercumulus augite, which is at variance with fractionation laws and led us to suggest that the rocks with cumulus pyroxenes were formed by a melt with a higher degree of fractionation than those of the intercumulus melts of the adjacent layers.

DOI: 10.1134/S0016702907020036

LINTRODUCTION

Systematic variations in the compositions of minerals interpreted in light of the crystallization differentiation theory reflect the evolution of magma during its solidification in a magmatic chamber. Magma crystallization and the settling of solid phases from it are coupled with changes in the composition of the residual melt due to the redistribution of components between the melt and newly formed minerals. Magma fractionation results, first of all, in a systematic crystallization sequence of minerals and a change in the cumulus mineral assemblage depending on the composition of the parental melt [1]. The first mineral to crystallize in layered intrusions is usually olivine (it is assumed that emplaced magmas contain intratelluric olivine crystals), which is followed by various lower-temperature minerals and mineral assemblages (depending on the composition of the parental melt). The crystallization of mineral assemblages is, in turn, associated with a systematic change in the composition of cotectic minerals (compositional layering): an increase in the #Fe of the pyroxenes and a decrease in the #Ca of the plagioclase. Compositional layering is thought to play a particularly important part in the cyclical intercalating rocks of layered massifs. The nature of the cyclicity is still a debatable issue, and, as of now, about 20 hypotheses were put forth to explain the genesis of the rhythmicity in layered intrusions [2]. Compositional variations in the minerals can serve as indicators of variations in the crystallization conditions, and the interpretations of the tendencies observed in these variations provide grounds to validate or invalidate certain petrological hypotheses.

Several papers were devoted to the complex study of layered series, including the compositional layering [3–6 and others]. Analysis of these materials indicates that, although the inner structures of layered massifs show general similarities, the structure of their rhythmically layered units often display certain individual features in each of the intrusions. Moreover, most earlier papers on these bodies reported data on units with ore mineralization and only scarce information on small portions of the layered series (for example, [3] and others). Our research was centered on studying the systematic variations in the composition of rock-forming minerals of the whole Kivakka intrusion and on the more detailed examination of the chemistries of minerals composing the whole vertical section of the rhythmically intercalating meso- and melanocratic norites of the Norite Zone in the Kivakka intrusion.

GEOLOGY, SHAPE, AND INNER STRUCTURE OF THE KIVAKKA INTRUSION

The Kivakka intrusion in northern Karelia (Fig. 1) belongs to the Olanga group of layered peridotite–gabbro–norite intrusions, which are hosted by migmatized biotite and amphibole gneisses, granite-gneisses, and granodiorite-gneisses of Late Archean age [7, 8]. The Kivakka intrusion is an originally vertical inverted cone, whose axis was calculated to have been approximately 3900 m long and whose apex angle has been 80°. In its modern position, the axis of the intrusion dips northwest at an angle of approximately 40°, so that the upper part of the cone composed of the layered series (from the side—in fact, upper—chill zone to the roof) is exposed.

The Kivakka intrusion is anisotropic and layered. The apparent thickness of the massif in its central portion reaches ~2000 m. The massif was dated at 2420 ± 23 Ma (Sm–Nd) and 2444 ± 1 Ma (U–Pb) [9–11].

The large-scale stratigraphy of the Layered Series was based on the principle of cumulus mineral assemblages [7]. From bottom to top and according to the sets of cumulus minerals, the series was subdivided into olivinite, norite, gabbro-norite, and gabbro-norite with pigeonite zones (Fig. 1). When studying the rocks composing the Kivakka intrusion, we relied on the systematics of cumulus rocks, whose advantages in application to layered series are self-evident. The distinguishing of cumulus and intercumulus mineral assemblages in the rocks enabled us to unambiguously reveal the succession of liquidus associations in vertical sections of the intrusion.

The *Lower Contact Zone (LCZ)* is dominated by gabbro-norites (bronzite–plagioclase–augite cumulus assemblage) and has a thickness of no more than 100 m. In the vertical section (from bottom to top), the transition to the Layered Series is seen as intercalations with a reverse sequence of cumulus assemblages (from gabbro-norites to olivinites). The apparent thickness of the interlayered unit is 15 m.

The thickness of the Layered Series is approximately 1700 m.

The *Olivinite Zone (OZ)* composes the bottom part of the Layered Series. The predominant cumulus mineral in this zone is olivine (olivine cumulus assemblage). The OZ is about 400 m thick, and its uppermost 50 m contain much cumulus bronzite, which determines the transition to the Norite Zone through intercalations of harzburgite (olivine–bronzite assemblage) and bronzitites (bronzite assemblage). The thickness of the intercalation unit is 20–30 m. We think that the unexposed part of the cone is made up of olivinite.

The *Norite Zone* is as thick as 700 m, and its cumulus minerals are bronzite and plagioclase, with the diversity of the rocks determined largely by variations in the proportions of these minerals and their sizes. The predominant rocks are norites (bronzite–plagioclase cumulus assemblage). Below the level of 400 m, the Norite Zone consists of medium-scale rhythmic intercalations of melanocratic (bronzite assemblage) and meso- to leucocratic (bronzite–plagioclase assemblage) norites and is referred to as the Intercalation Subzone of Bronzitites and Norites, which is overlain by relatively homogeneous meso- and leucocratic norites. The Norite Zone hosts the richest units of low-sulfide PGE mineralization. The transition between the Norite and Gabbro-Norite zones occurs via a coarse intercalation of norites and gabbro-norites.

The *Gabbro-Norite Zone* consists mostly of gabbro-norites, which are made up of the three-mineral bronzite–plagioclase–augite cumulus assemblage and are relatively homogeneous. The thickness of this zone is close to 420 m.

The uppermost unit of the Layered Series is the *Gabbro-Norite Zone with Pigeonite* as a low-calcic pyroxene. Its thickness reaches 320 m. The rocks composing this zone only insignificantly differ in composition from the underlying gabbro-norites, but the cumulus orthopyroxene gives way to inverted pigeonite. The uppermost 50 m of this zone consist of rocks rich in titanomagnetite, biotite, potassic feldspar, and apatite.

This unit is overlain by the significantly epidotized rocks of the *Upper Contact Zone* ~50 m in thickness.

A detailed petrochemical characterization of rocks composing the intrusion was given in [7].

Judging from the succession of zones in the Layered Series corresponding to the succession of cumulus mineral assemblages in the vertical section of the intrusion, the chamber was filled with solid phases from bottom to top, in compliance with the following crystallization succession (Fig. 1): olivine $\longrightarrow$ (– olivine) + orthopyroxene $\longrightarrow$ orthopyroxene + plagioclase $\longrightarrow$ orthopyroxene + plagioclase + clinopyroxene $\longrightarrow$ (– orthopyroxene) + clinopyroxene + plagioclase + pigeonite (the minus sign denotes the incongruent dissolution of a phase).

The transitions between the zones are marked by intercalations of rocks consisting of various cumulus assemblages: those composing the underlying zone and those crystallizing according to the crystallization sequence specified above. The most contrasting intercalations occur in the transition zone from the olivinite to norite zones, namely, in the unit of intercalating melanocratic norite (bronzite cumulate) and meso- and leucocratic norite (bronzite–plagioclase cumulate). The sharp boundaries are readily discernible, and the specific geomorphologic features (cuestas) facilitate tracing the layers through the whole intrusion.

SPATIAL CHARACTERISTICS OF THE RHYTHMIC LAYERING IN THE SUBZONE OF INTERCALATING BRONZITITES AND NORITES

The Subzone of Intercalating Bronzitites and Norites (SIBN) has a thickness of approximately 400 m

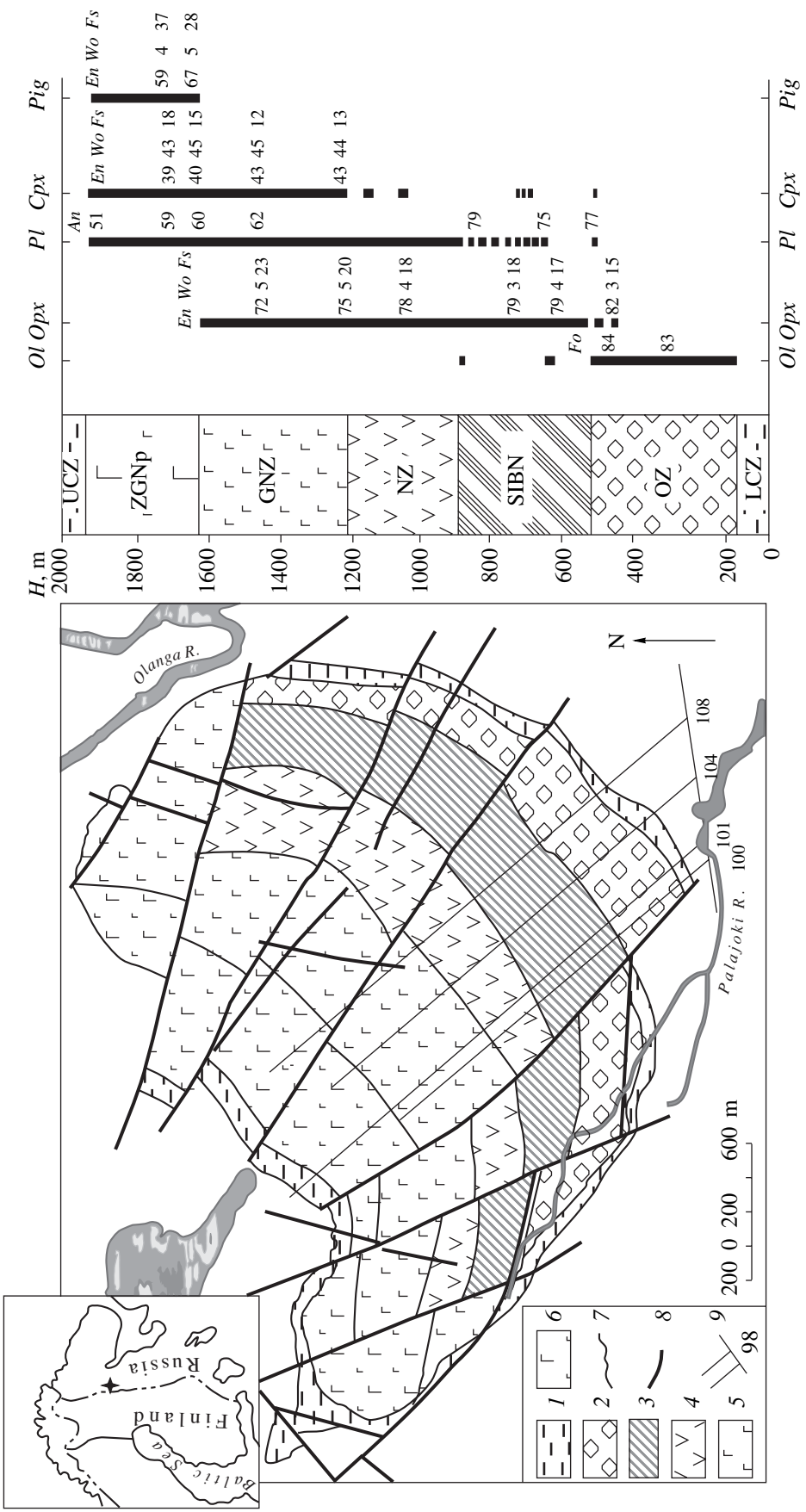

Fig. 1. Schematic geological map of the Kivakka intrusion and the vertical section of this intrusion with the distribution of cumulus minerals. (*1*) Lower and Upper Contact Zones (LCZ and UCZ, respectively); (*2*) Olivinite Zone (OZ); (*3*, *4*) Norite Zone (NZ); (*3*) Subzone of Intercalating Bronzitites and Norites (SIBN); (*5*) Gabbro-Norite Zone (GNZ); (*6*) Zone of Gabbro-Norites with Pigeonite (ZGNp); (*7*) geologic boundaries; (*8*) faults; (*9*) profiles of YUKE PGO Sevzapgeologiya.

Minerals: *Ol*—olivine; *Opx*—low-Ca orthopyroxene; *Pl*—plagioclase; *Cpx*—high-Ca clinopyroxene; *Pig*—pigeonite.

and composes the bottom of the Norite Zone. Its lowermost part consists of pyroxenites and melanocratic norites, which crown the transition zone from the Olivinite to the Norite Zone through a unit of intercalating harzburgite and bronzitite. The SIBN is made up mostly of melano-, meso-, and leucocratic norites with subordinate amounts of gabbro-norites [12]. The contrasting character of the intercalation is determined by alternating melanocratic rocks with 10–15% plagioclase and meso- and leucocratic norites and gabbro-norites with 40–80% plagioclase.

The units of cyclic intercalations distinguished in the vertical section [12] consist of meter-scale layers. The upper and lower parts of the cyclic units are conventionally determined as follows: the bottom of a unit consists of rocks composed of a cumulus assemblage produced by less fractionated melt.

The *bottom part* of each cyclic unit is made up of a layer of relatively homogeneous medium-grained melanocratic norite (bronzite cumulate) a few meters thick. The rocks consist of euhedral and subhedral orthopyroxene crystals (from 65 to 85% of the rocks, 80% on average), anhedral plagioclase grains (5–15%), and augite oikocrysts (<5%). These rocks are readily weathered and give rise to a characteristic hilly surface topography. The melanocratic norites are easily identified in field, are characterized by a systematic position in the vertical section, and have sharp boundaries with the under- and overlying norites and gabbro-norites.

The *upper part of the cyclic units* is composed of meso- and leucocratic norites and gabbro-norites (bronzite–plagioclase and bronzite–plagioclase–augite cumulates, respectively). Their thicknesses vary from a few meters to a few dozen meters. The rocks are highly heterogeneous and show centimeter-scale layering, variable grain sizes, trachytic textures, and other structural and textural heterogeneities. The mesocratic and leucocratic norites consist of subhedral crystals of plagioclase (35–85%) and orthopyroxene (30–60%) and contain oikocrysts of clinopyroxene (<5%). The gabbro-norites composing the upper parts of four cyclic layers consist of subhedral plagioclase (50–70%), orthopyroxene (10–30%), and clinopyroxene (10–20%).

The SIBN was subdivided into 18 rhythmic units (Fig. 2) and is crowned by a thick layer of coarse-grained melanocratic norites (bronzite cumulate).

Unexpectedly, the SIBN includes gabbro-norites with cumulus clinopyroxene, which compose the upper parts of cyclic units 4, 5, 6, and 8 (persistent occurrence of the bronzite–plagioclase–augite assemblage was detected only 500 m higher in the vertical section, in the Gabbro-Norite Zone). The inner structures of the cyclic units remain consisting of two rock types: the bottom parts composed of melanocratic norites (bronzite cumulates), whose composition and structures are analogous to the melanocratic norites of the whole rhythmically layered series, and the tops composed of gabbro-norites (in the absence of the transitional bronzite-plagioclase assemblage, which corresponds to the crystallization sequence).

The data obtained on boundaries between the cycles and layers within a single cycle reveal a sharp change in the mineral proportions at layer boundaries (Fig. 2), and, as can be seen in thin sections, the textural patterns of the rocks also drastically change. It is particularly interesting to examine the boundary between the melanocratic norites and overlying gabbro-norites: the websterite assemblage appears in the melanocratic layer immediately above this boundary (within 0.5 m), with ortho- and clinopyroxene as the cumulus minerals.

METHODS

Calculation of the Optimum Number of Microprobe Measurements Needed to Determine the Composition of Minerals

In order to characterize the variability of mineral chemistries in the vertical section of the intrusion, rock samples were collected at boundaries between megacycles [7]. In the rhythmically layered portion of the vertical section, we analyzed cumulus grains of bronzite, augite, and plagioclase. Five bronzite and three augite and plagioclase grains of the most euhedral habit were separated from each of the samples.

The minerals were analyzed on a Camebax-microbeam (Cameca) microprobe at the Vernadsky Institute of Geochemistry and Analytical Chemistry, Russian Academy of Sciences (analyst N.N. Kononkova). The accelerating voltage was 15 kV, and the counting time for major components was 20 s. The analytical lines were the K_α series of corresponding elements. The standard for most major components was Augite no. 172142; albite was used as the standard for Na, $MnTiO_3$ as the standard for Ti and Mn, and Cr_2O_3 as the standard for Cr.

First of all, the grains were examined for the presence of compositional zoning. For this purpose, microprobe profiles were run across a few grains along their longer axes. No zoning was detected in the grains of ortho- and clinopyroxene.

The occurrence of exsolution textures in the pyroxenes (these textures are typical of the minerals) made it notably more difficult for us to estimate the bulk composition of the grains, because the excitation spots of the microprobe beam could include random proportions of lamella and matrix material. It is expedient to know beforehand the number of analyses and their regime needed to characterize a phase and the character of its exsolution within a single sample with a needed accuracy. Difficulties can be encountered when the concentrations of such trace elements as Cr are determined, because the accuracy of the analytical technique is insufficient at low concentrations of an element to be determined (the precision of the analyses is commensurable with the natural dispersion of the concentrations and equals 0.2 wt %).

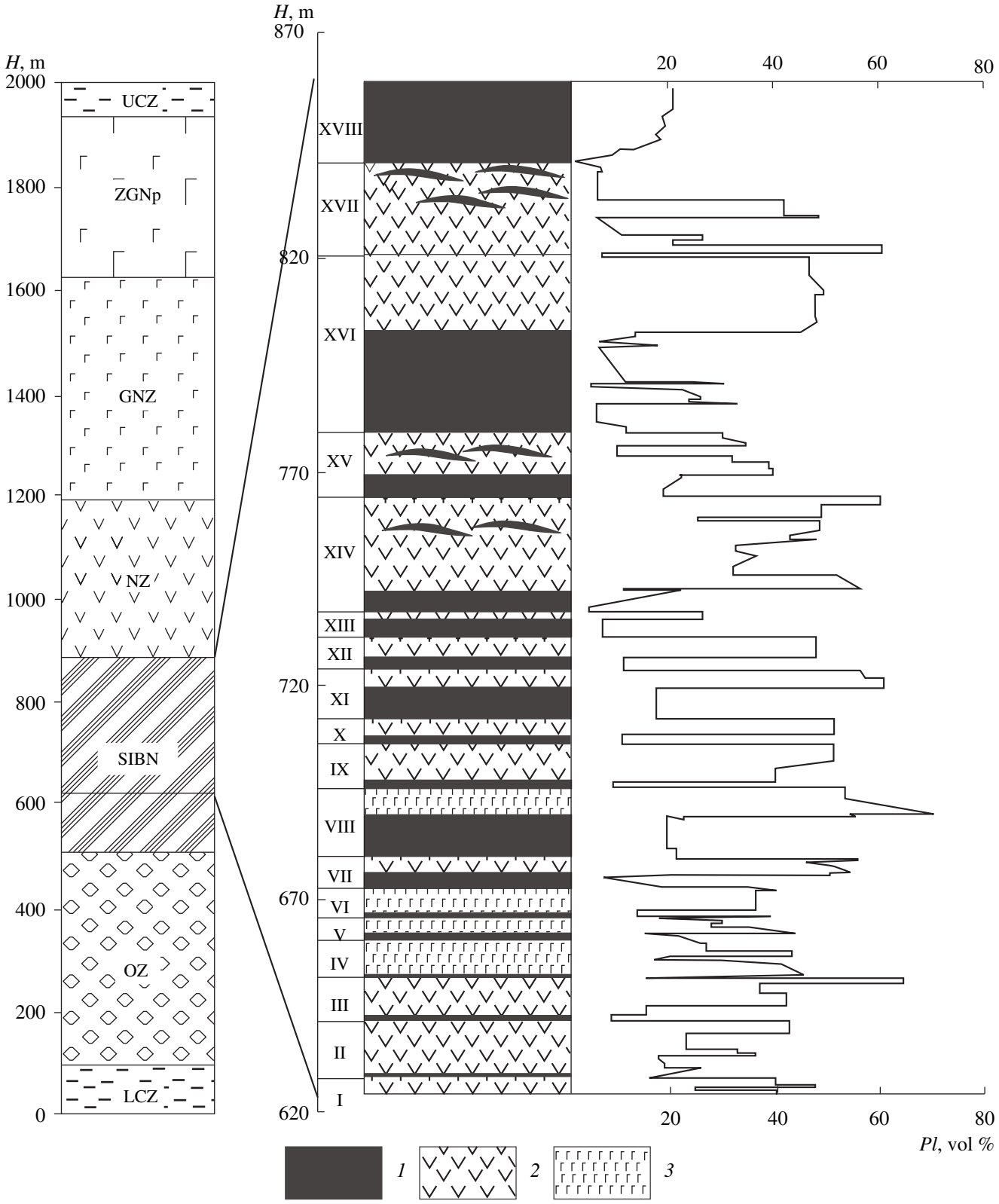

Fig. 2. Vertical section through the zone of contrasting intercalations and plagioclase contents in the rocks (calculated from rock densities). (*1*) Bronzite cumulate; (*2*) bronzite–plagioclase cumulate; (*3*) bronzite–plagioclase–augite cumulate. Roman numerals correspond to the rhythmic units recognized in the vertical section. See Fig. 1 for other symbol explanations.

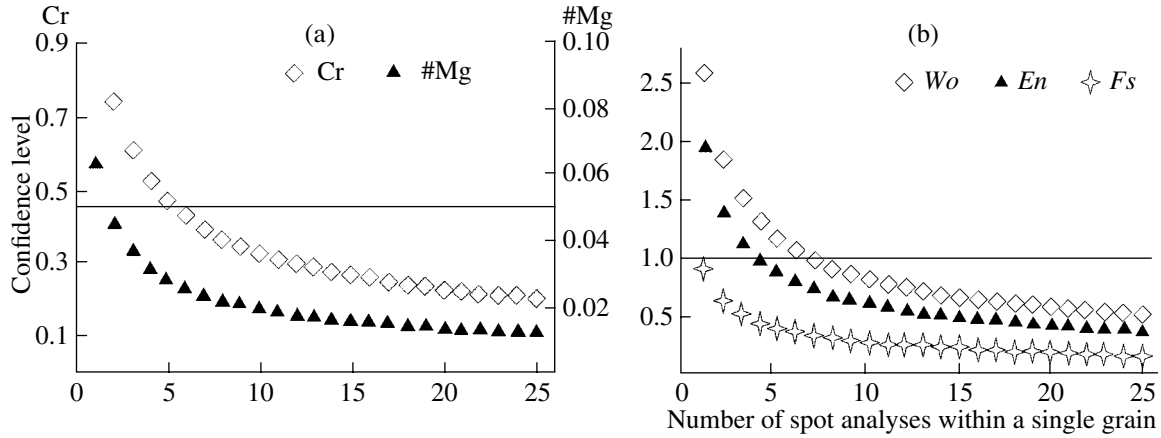

Fig. 3. Determination of the number of analyses with a specified confidence level needed to accurately assay the composition of orthopyroxene: (a) #Mg and Cr, (b) *En*, *Fs*, and *Wo* concentrations.

In view of these considerations, we have conducted a specialized methodical research with the aim of determining the minimum number of analyses within a single grain required for the determination of the major- and trace-element composition of a mineral with the required accuracy. One orthopyroxene and one clinopyroxene grain were analyzed at 64 spots each (which is equal to the maximum possible number of microprobe analyses to be conducted during a single working shift at the microprobe) at randomly selected spots. The analyses thus obtained were utilized to calculate the average values, standard deviations, and confidence level for #Mg = MgO/(MgO + FeO) and for the concentrations of end members and trace elements.

It was determined that #Mg values can be obtained with a 95% confidence level (within ±0.005 of the averages) using only three analyses for orthopyroxene (Fig. 3a) and as many as 60 analyses for clinopyroxene (Fig. 4a). Reliable values for the *Wo* end member (within ±1) can be derived for orthopyroxene from eight spot analyses within a single grain (Fig. 3b). At the same time, the *En* and *Fs* end members can be determined accurately enough based on only three spot analyses. An acceptable accuracy of *Wo* estimates for clinopyroxene can be reached based on more than 64 analyses (Fig. 4b).

Reliable Cr concentrations (95% confidence level, accurate to ±0.04 wt %) can be determined by eight analyses within a single grain for orthopyroxene (Fig. 3a) and no less than 30 analyses for clinopyroxene (Fig. 4a).

It was thus determined that the method of an increase in the number of analyses and the calculation of average values of three analyses for #Mg and of eight analyses for Cr is optimal for orthopyroxene and provides means for a detailed economic solution of the problem. At the same time, this method was proved inapplicable to clinopyroxene, because its exsolution

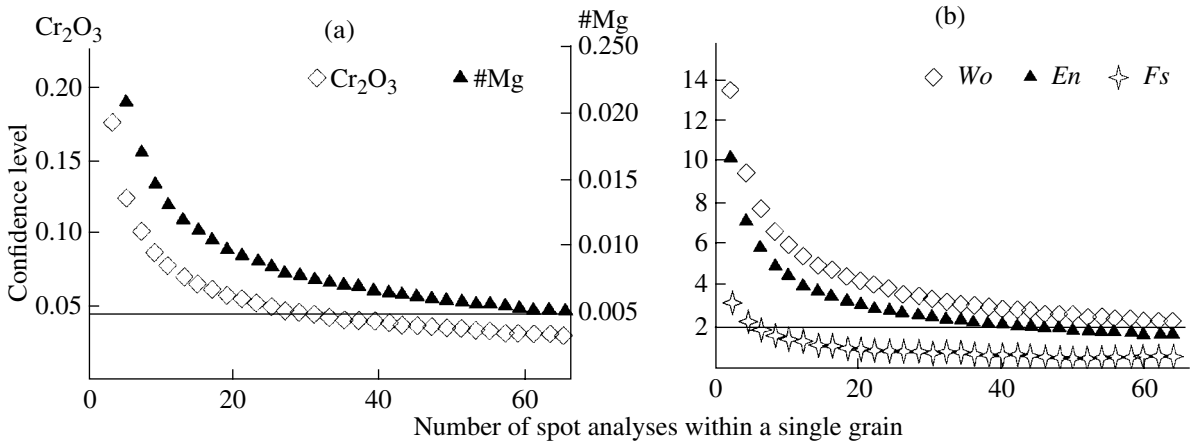

Fig. 4. Determination of the number of analyses with a specified confidence level needed to accurately assay the composition of clinopyroxene: (a) #Mg and Cr_2O_3, (b) *En*, *Fs*, and *Wo* concentrations.

lamellae are coarser, and their composition must be taken into account.

With regard for the composition and amount of exsolution lamellae in clinopyroxene grains, we calculated them in cumulus and intercumulus augite grains. For this purpose, we selected grains with the best pronounced exsolution textures (within a single thin section) and examined two areas in each of the grains. The back scattered electron (BSE) images of these areas displayed orthopyroxene lamellae (whose composition significantly differed from the matrix augite in having lower CaO concentrations, Fig. 5). The sharp boundaries of the lamellae allowed us to easily distinguish between the matrix and exsolved materials. A significant disadvantage of computerized appraising of the areas of various composition (various color) is that this method takes into account halftones that are caused by the uneven surface of the material and cracks in the mineral grain. Because of this, we calculated the relative volumes of the phases manually. In BSE images, we drew profiles across lamellae with a step close to the average distance between the exsolution lamellae. The matrix/lamella proportions in the clinopyroxene were determined to be practically the same in all of the grains, regardless of their genesis, and equaled 86/14. This led us to conclude that the amount of the exsolution lamellae remains constant in all pyroxene grains, and hence, the composition of a clinopyroxene grain before its exsolution can be easily calculated if the compositions of the matrix and lamellae are known. Our statistical data indicate that the contents of the *Wo* end member in the clinopyroxene matrix remain notably varying even when calculated in this manner, and this parameter can be calculated accurate to ±0.01 from no less than six spot analyses, whereas the composition of the lamellae almost does not vary and can be calculated from three spot analysis. The Cr concentration can be calculated accurate to ±0.06 wt % from three analyses for a lamellae and six for the matrix.

Recalculation of Plagioclase Compositions into End Members (Ab and An)

The composition of plagioclase was calculated into its end members (*Ab* and *An*) by six various techniques, using the proportional of various elements and the following simple stoichiometric relations:

$$An_{\mathrm{CaNa}} = \frac{\mathrm{Ca}}{\mathrm{Ca+Na+K}} \times 100,$$

$$An_{\mathrm{CaSi}} = \frac{2\mathrm{Ca}}{\mathrm{Ca+Si}} \times 100,$$

$$An_{\mathrm{CaAl}} = \frac{\mathrm{Ca}}{\mathrm{Al-Ca}} \times 100,$$

$$An_{\mathrm{AlNa}} = \frac{\mathrm{Al-Na-K}}{\mathrm{Al+Na+K}} \times 100,$$

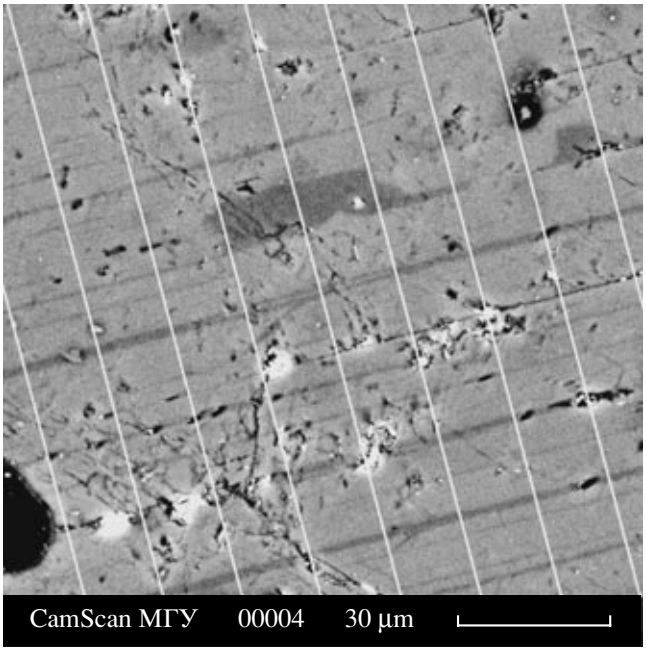

Fig. 5. BSE image of a clinopyroxene grain with profiles (white lines) along which the proportions of the matrix and lamella material were calculated.

$$An_{\mathrm{AlSi}} = \frac{3\mathrm{Al-Si}}{\mathrm{Al+Si}} \times 100,$$

$$An_{\mathrm{SiNa}} = \frac{\mathrm{Si}-3(\mathrm{Na+K})}{\mathrm{Si}-(\mathrm{Na+K})} \times 100.$$

The six calculated compositions were combined in threes with the participation of the same element. If the differences between the calculated end-member contents within a group of three were significant, the values calculated using these elements were rejected from the set. The remaining three were used to calculate an average value, which was considered the most reliable. This fairly complicated procedure was applied because elements contained in plagioclase cannot always be equally good determined by a microprobe, and thus, the most "problematic" elements, which introduced a significant dispersion, were rejected.

COMPOSITION OF ROCK-FORMING MINERAL OF THE KIVAKKA INTRUSION

The major rock-forming minerals of the Kivakka intrusion are olivine, low-Ca orthopyroxene, high-Ca clinopyroxene (augite), pigeonite, and plagioclase. All of them display compositional variations, and their compositional trends can provide direct information on the crystallization succession of the rocks composing the massif.

Olivine is the only cumulus mineral of the olivinites and accounts for up to 80% of these rocks by volume.

The composition of the olivine corresponds to chrysolite (82–85 mol % of the forsterite end member). Our data on the composition of the olivine demonstrate its high local homogeneity, with some variations in the *Fo* concentration within individual grains (within 2 mol %) reflecting weak crystallization zoning. The differences in the average compositions of the olivine depending on its position in the vertical section of the intrusion are within the geochemical and analytical dispersions and are statistically insignificant.

Low-Ca orthopyroxene is the most widely spread mafic mineral in rocks of the massif and is contained in various textural groups. Because of this, the mineral is of the most interest as carrying information on the melt evolution during the development of the Kivakka Massif. The composition of the orthopyroxene widely varies (from 54 to 83 mol % *En*) and corresponds mostly to bronzite, although the rocks of the lower contact zone and the gabbro-norites of the upper part of the Layered Series contain hypersthene. The average contents of the wollastonite end member in the orthopyroxene do not exceed 4–5 mol % (Table 1).

Within each sample, the *En* contents of the orthopyroxene of the first textural group vary within 5–8 mol %. The average chemical composition of the orthopyroxene systematically varies in the vertical section of the massif and provides a principal record of the compositional evolution of the melt during the crystallization differentiation of the massif. This can be most clearly seen in the variations in the #Mg in Fig. 6 (its decrease up the vertical section of the massif). The composition of the intercumulus orthopyroxene of textural group II in the olivinites is quite magnesian. The average composition of the first cumulus orthopyroxene in the bronzitites and norites in the lower part of the intercalation unit corresponds to typical bronzite (approximately 80 mol % *En*) and varies little within this unit. The composition of the orthopyroxene of the norites and gabbro-norites gradually becomes less and less magnesian.

High-Ca clinopyroxene is a relatively widely spread mafic mineral in the rocks of the massif and was found in practically all rock varieties as a member of various textural groups. This mineral is contained in accessory amounts in the olivinites and in minor amounts in the bronzitites and norites, in which it is a mineral of the second textural group. Its composition generally corresponds to augite with 42–48% of the wollastonite end member and 40–48% of the enstatite end member (Table 1).

The composition of augite somewhat varies within a single sample (for example, the enstatite concentrations may vary within 2–4 mol %). The #Mg of augite systematically decreases up the vertical section of the massif, but the compositions of this mineral changes slowly before pigeonite appears in the rocks. In the zone of gabbro-norites with pigeonite, the #Mg of the clinopyroxene decreases by 0.25 (Fig. 6).

Similarly to the orthopyroxene, the augite in the gabbro-norites in the lower contact zone has a somewhat lower #Mg. The composition of intercumulus augite of textural group II in the olivinites and bronzitites is fairly magnesian and corresponds to the composition of normative pyroxene component in these rocks.

Pigeonite appears as a rock-forming mineral in the upper part of the Kivakka Massif. The mineral always occurs as grains inverted via the exsolution of the solid solution into an orthopyroxene phase and augite, which makes it much more difficult to estimate the bulk composition of the grains corresponding to pigeonite in equilibrium with melt. Our scarce spot analyses (including a few analyses by a defocused beam) display broad variations in the concentration of the wollastonite end member and also indicate that no individual spot analyses can be representative. The compositions of the orthorhombic and monoclinic phases in pigeonite grains correspond to those of hypersthene and augite in the rocks containing the pigeonite.

Plagioclase is a major or minor (accessory) mineral in practically all rocks composing the massif and is contained in variable textural groups. Its composition broadly varies (the anorthite concentrations vary from 50 to 80 mol %) and corresponds to labradorite-bytownite (Table 2).

In each rock (thin section), the composition of plagioclase notably varies (within 10–12 mol % anorthite), reflecting crystallization zoning and the affiliation of individual grains to different textural groups.

The composition of plagioclase in textural group II in the olivinites is close to the composition of the mineral in the rocks of the lower contact zone and corresponds to the normative composition of the plagioclase component in the weakly fractionated interstitial melt.

With the transition to the rocks of the intercalation zone, whose norites contain plagioclase as a major rock-forming mineral of the cumulus assemblage (minerals of textural group I), the composition of plagioclase becomes much more calcic, up to 78–79 mol % anorthite (in compliance with the crystallization tendencies). This drastic change in the plagioclase composition definitely testifies that this is a cumulus mineral of the norites. A significant compositional evolution of plagioclase is typical of the upper part of the vertical section (in the gabbro-norites and gabbro-norite with pigeonite), in which the anorthite content of plagioclase gradually deceases up the vertical section (Fig. 6).

COMPOSITION OF ROCK-FORMING MINERALS IN THE SUBZONE OF INTERCALATING BRONZITITES AND NORITES

The study of the compositions of rock-forming minerals from the Subzone of Intercalating Bronzitites and Norites was an important part of the examination of contrasting intercalations in the central part of the Kivakka Massif. The compositions of the rock-forming

Table 1. Composition of pyroxene in the vertical section of the Kivakka intrusion

Component	low-Ca pyroxene											
	KV-403*		KV-418		KV-419		KV-420		KV-424		KV-426	
	140**		468		506		526		612		655	
	ave. of (6)***	conf. lev.	ave. of (6)	conf. lev.	ave. of (5)	conf. lev.	ave. of (4)	conf. lev.	ave. of (6)	conf. lev.	ave. of (6)	conf. lev.
SiO_2	55.71	0.690	55.53	0.739	56.47	0.488	55.73	0.684	55.82	0.363	56.54	0.673
TiO_2	0.12	0.017	0.29	0.167	0.14	0.011	0.16	0.020	0.15	0.036	0.14	0.017
Al_2O_3	2.68	0.169	2.60	0.252	2.12	0.090	2.58	0.073	2.59	0.155	2.62	0.151
FeO	9.61	0.261	10.26	0.175	10.29	0.451	10.01	0.313	10.42	0.168	10.20	0.238
MnO	0.22	0.029	0.22	0.020	0.24	0.023	0.24	0.033	0.25	0.031	0.24	0.033
MgO	28.80	0.453	30.08	0.439	29.11	0.559	28.83	0.449	27.91	0.400	29.01	0.460
CaO	2.08	0.504	1.33	0.244	2.79	0.747	1.88	0.486	1.99	0.372	1.69	0.565
Na_2O	0.08	0.043	0.03	0.022	0.03	0.016	0.04	0.029	0.06	0.013	0.04	0.019
Cr_2O_3	0.47	0.039	0.44	0.067	0.29	0.082	0.55	0.040	0.58	0.049	0.45	0.040
Total	99.93	0.832	100.79	0.864	101.47	0.674	100.02	0.987	99.92	0.824	100.91	0.875
En	15.91	0.418	81.49	0.726	78.61	0.952	80.23	0.742	79.11	0.583	80.41	0.809
Fs	80.42	0.661	15.95	0.346	15.97	0.595	16.01	0.350	16.86	0.187	16.23	0.434
Wo	4.18	1.003	2.58	0.492	5.41	1.477	3.75	0.980	4.02	0.715	3.36	1.104
#Mg	0.84	0.003	0.84	0.004	0.83	0.004	0.84	0.003	0.83	0.003	0.84	0.003

Component	KV-430		KV-446		KV-452		KV-465		KV-475		KV-477	
	748		1080		1200		1458		1665		1707	
	ave. of (6)	conf. lev.	ave. of (6)	conf. lev.	ave. of (6)	conf. lev.	ave. of (6)	conf. lev.	ave. of (6)	conf. lev.	ave. of (2)	conf. lev.
SiO_2	56.23	0.401	56.10	0.312	55.45	0.347	55.90	0.130	54.05	0.769	53.43	0.333
TiO_2	0.17	0.048	0.19	0.040	0.17	0.045	0.22	0.060	0.18	0.042	0.33	0.029
Al_2O_3	2.23	0.113	2.00	0.084	1.87	0.190	1.37	0.100	1.46	0.116	1.41	0.069
FeO	10.91	0.276	11.68	0.130	12.85	0.361	14.54	0.487	17.69	0.655	21.26	0.519
MnO	0.20	0.026	0.25	0.050	0.27	0.041	0.30	0.024	0.35	0.047	0.47	0.000
MgO	27.91	0.302	28.83	0.651	27.95	0.623	25.48	0.246	24.96	0.756	23.47	0.549
CaO	1.59	0.242	1.59	0.509	1.97	0.804	1.71	0.583	2.29	0.141	1.14	0.078
Na_2O	0.02	0.021	0.01	0.014	0.04	0.018	0.02	0.022	0.02	0.013	0.01	0.020
Cr_2O_3	0.48	0.035	0.43	0.016	0.26	0.053	0.11	0.042	0.02	0.019	0.03	0.029
Total	99.90	0.469	101.09	0.823	100.86	0.696	99.65	0.169	100.96	0.844	101.53	0.892
En	79.10	0.343	78.61	0.874	76.06	1.215	72.73	0.577	68.01	1.362	64.33	0.059
Fs	17.63	0.378	18.26	0.298	20.08	0.496	23.77	0.701	27.60	1.221	33.43	0.029
Wo	3.24	0.505	3.14	0.987	3.87	1.614	3.51	1.201	4.39	0.274	2.25	0.088
#Mg	0.82	0.003	0.81	0.003	0.79	0.002	0.76	0.005	0.72	0.013	0.66	0.000

Component	low-Ca pyroxene		high-Ca pyroxene							
	KV-478		KV-18/7		KV-403		KV-419		KV-426	
	1727		100		140		506		655	
	ave. of (7)	conf. lev.	ave. of (4)	conf. lev.	ave. of (5)	conf. lev.	ave. of (2)	conf. lev.	ave. of (4)	conf. lev.
SiO_2	53.06	0.435	52.01	0.477	52.70	0.388	52.80	1.156	53.53	0.843
TiO_2	0.33	0.042	0.37	0.017	0.35	0.019	0.30	0.049	0.42	0.033
Al_2O_3	1.25	0.242	3.06	0.074	3.95	0.098	3.51	0.000	3.96	0.102
FeO	23.29	0.360	7.55	0.212	5.09	0.103	5.16	0.402	4.89	0.093
MnO	0.53	0.12	0.22	0.045	0.18	0.031	0.18	0.029	0.16	0.043
MgO	21.25	0.642	14.72	0.042	15.86	0.422	16.23	0.245	15.69	0.348
CaO	1.93	0.703	21.55	0.419	22.46	0.261	21.91	0.000	22.21	0.270
Na_2O	0.03	0.014	0.43	0.048	0.49	0.012	0.40	0.010	0.44	0.038
Cr_2O_3	0.01	0.016	0.25	0.052	0.51	0.070	0.48	0.137	0.81	0.031
Total	101.71	0.484	100.14	0.624	101.40	0.349	100.97	1.117	102.12	0.587
En	59.01	1.657	42.44	0.246	45.05	0.319	46.41	0.647	45.49	0.608
Fs	37.13	0.695	12.59	0.370	8.52	0.202	8.54	0.608	8.23	0.267
Wo	3.86	1.403	44.96	0.524	46.43	0.317	45.05	0.039	46.28	0.610
#Mg	0.62	0.010	0.78	0.005	0.85	0.006	0.85	0.012	0.85	0.004

Table 1. (Contd.)

Component	high-Ca pyroxene							
	KV-430		KV-466		KV-475		KV-478	
	748		1477		1665		1727	
	ave. of (3)	conf. lev.	ave. of (6)	conf. lev.	ave. of (2)	conf. lev.	ave. of (2)	conf. lev.
SiO_2	53.32	0.571	51.89	0.528	52.54	0.137	51.82	1.137
TiO_2	0.34	0.120	0.41	0.079	0.75	0.206	0.59	0.118
Al_2O_3	3.82	0.225	2.70	0.563	2.61	0.118	2.81	0.029
FeO	5.57	0.818	6.95	0.181	8.95	0.049	10.65	0.186
MnO	0.20	0.079	0.21	0.037	0.22	0.010	0.31	0.029
MgO	16.47	0.972	15.13	0.177	13.76	0.431	13.34	0.216
CaO	20.61	2.111	21.66	0.337	21.51	0.274	20.42	0.402
Na_2O	0.38	0.102	0.27	0.031	0.28	0.029	0.36	0.020
Cr_2O_3	0.74	0.122	0.19	0.238	0.02	0.029	100.34	1.068
Total	101.46	0.171	99.41	0.511	100.61	0.843	0.06	0.020
En	47.70	2.860	43.58	0.387	40.04	0.568	39.05	0.568
Fs	9.39	1.458	11.58	0.341	14.97	0.363	18.00	0.343
Wo	42.91	4.257	44.84	0.470	45.01	0.206	42.95	0.902
#Mg	0.84	0.014	0.79	0.006	0.73	0.007	0.69	0.000

* Sample no.

** Position in the vertical section (m).

*** Average of the number of analyses specified in parentheses; conf. lev. is the confidence level.

minerals were determined on a microprobe in 950 grains sampled from the bottom, intermediate, and upper parts of the melanocratic and mesocratic layers of each rhythmic unit. Two cycles were sampled with a step of 0.5 m in the mesocratic layer and 0.2 m in the melanocratic layer to obtain more detailed characteristics of mineral chemistries within this cycle.

Low-Ca orthopyroxene (bronzite) is the only mineral contained in all of the cumulus assemblages sampled in this portion of the vertical section. Our data on the compositions of orthopyroxene grains indicate that they have no zoning.

Microprobe analyses of bronzite grains demonstrate that the composition of the mineral practically does not change throughout the whole vertical section and corresponds to $En_{77–79}$ on average. In a *Wo–En–Fs* diagram (Fig. 7), the compositions show an insignificant (within 3%) shift along the *En–Fs* join.

The variation range of the #Mg of the bronzite in the vertical section of the intrusion is 0.03–0.04 and does not exceed the dispersion of the #Mg within a single sample. Insignificant variations in the #Mg were also observed within individual rhythmic units, in spite of the differences between the compositions of the cumulus assemblages of adjacent layers. The #Mg distribution within the rhythmic units does not show either the typical patterns that were extensively described in the literature and that reflect a decrease in #Mg from the bottom to tops of individual cycles and an abrupt increase in the bottom part of the overlying rhythmic unit (see, for example, [3, 13, 14]) or any statistically significant variations in the #Mg of orthopyroxene in the vertical section (Fig. 8a). Neither did we detect any significant variations in the concentrations of other major components (Table 3).

Inasmuch as the concentrations of oxides contained in orthopyroxene are commonly quite constant, we paid much attention to the Cr concentrations in the bronzite, because the Cr distribution coefficient of orthopyroxene is close to 5 (judging from the experimental data in [15]), and thus, the relative Cr concentration in this mineral can be used as a quantitative criterion of the fractionation of the magma that produced the layers. Accommodated as a minor component in pyroxenes, Cr is gradually depleted in the melts during the crystallization of ortho- and, particularly, clinopyroxene, and hence, the concentrations of this element in the minerals are a measure of the degree of melt fractionation.

The analysis of Cr distribution reveals variations in its concentrations in the orthopyroxene of the bronzite, bronzite–plagioclase, and bronzite–plagioclase–augite cumulates that do not exceed the limits of the confidence levels (Table 4). Nevertheless, the Cr concentrations in bronzite from the mesocratic norites and gabbro-norites are systematically lower than in bronzite from the melanocratic norites (Fig. 8a).

High-Ca clinopyroxene in the rocks of the layered unit is augite. We analyzed cumulus augite from the upper parts of cycles 4–6 and 8 and from the intercumulus material of the same cycles.

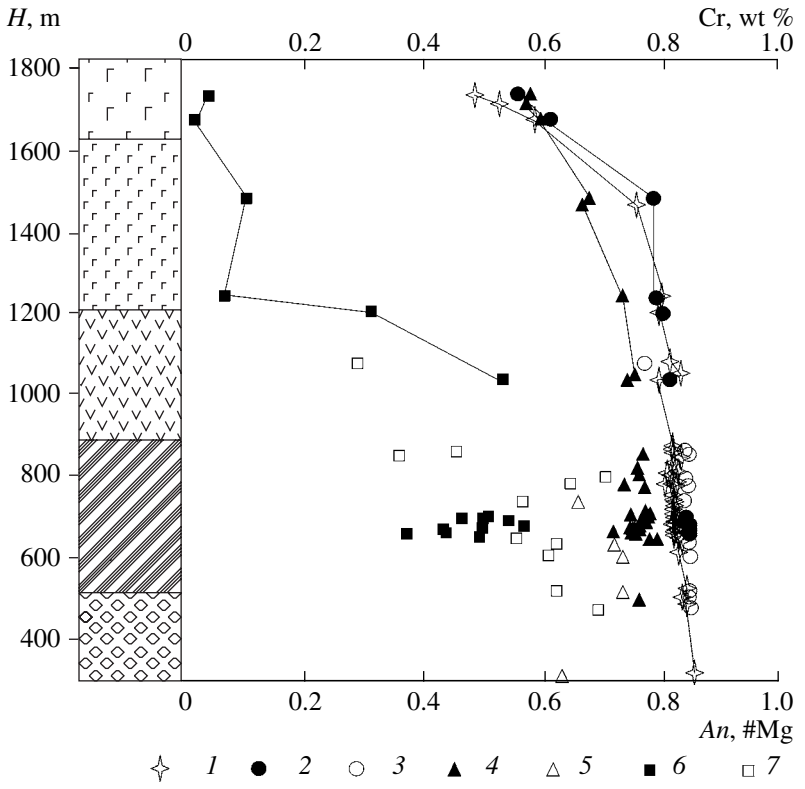

Fig. 6. Variations in the composition of minerals in the vertical section of the Kivakka intrusion. (*1*) #Mg of orthopyroxene; (*2*, *3*) #Mg of clinopyroxene: (*2*) cumulus crystals, (*3*) intercumulus crystals; (*4*, *5*) *An* content in plagioclase: (*4*) cumulus crystals, (*5*) intercumulus crystals; (*6*, *7*) Cr concentrations in clinopyroxene: (*6*) cumulus crystals, (*7*) intercumulus crystals.

The chemical composition of the clinopyroxene indicates that the #Mg of the augite practically does not vary in the vertical section, similarly to the analogous parameter of the orthopyroxene (Table 5, Fig. 8b). No zoning was detected in clinopyroxene grains.

The Cr concentrations in the clinopyroxene are notably different in these minerals from the cumulus and intercumulus grains in adjacent layers (Fig. 8b). The Cr concentrations in the cumulus augite varies from 0.38 to 0.6%. In the layers examined in much detail, we detected a decrease in the Cr contents in the central parts of the layers and an increase toward layer boundaries. This tendency is the most conspicuous in the central portion of the gabbro-norites of cycle 4, in which the Cr concentration decreases to 0.38%. The Cr contents somewhat increase (to 0.5%) in cycles 5, 6, and 8. Comparing these values with the concentrations determined in the vertical section, one can note analogous Cr concentrations in the bottom part of the Gabbro-Norite Zone of the intrusion some 500 m higher in the vertical section (Fig. 6).

The Cr concentrations in intercumulus clinopyroxene from the bronzite cumulates adjacent to gabbro-norite layers are not lower but even higher than in the cumulus mineral (0.60–0.70%, Fig. 8b). This suggests that the Cr content in the intercumulus melt in the bronzite cumulates was higher than in the melt from which the adjacent gabbro-norites crystallized.

Plagioclase is a cumulus mineral in the upper parts of all distinguished rhythmic units (i.e., meso- and leucocratic norites and gabbro-norites).

Our data indicate that the composition of the plagioclase varies from An_{70} to An_{80} (Table 6). Compositional variations were observed in individual grains of this

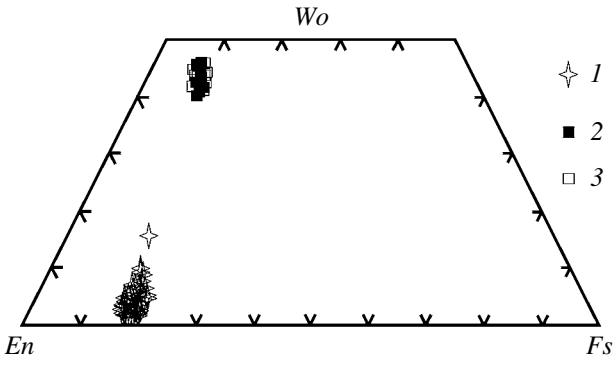

Fig. 7. *En–Fs–Wo* diagram for the compositions of pyroxene from the rhythmic intercalation subzone: (*1*) orthopyroxene; (*2*) cumulus clinopyroxene; (*3*) intercumulus clinopyroxene.

Table 2. Composition of plagioclase in the vertical section of the Kivakka intrusion

Component	KV-18/7*		KV-419		KV-420		KV-424		KV-426		KV-430	
	100**		506		526		612		655		748	
	ave. (11)***	conf. lev.	ave. (7)	conf. lev.	ave. (6)	conf. lev.	ave. (5)	conf. lev.	ave. (7)	conf. lev.	ave. (3)	conf. lev.
SiO_2	54.18	0.268	49.10	0.452	48.25	0.358	48.42	0.662	47.81	0.346	51.21	0.968
Al_2O_3	29.55	0.235	33.06	0.347	32.10	0.202	32.49	0.597	33.61	0.332	31.87	0.098
FeO	0.39	0.020	0.33	0.041	0.28	0.041	0.26	0.030	0.36	0.030	0.28	0.020
CaO	11.96	0.345	15.62	0.692	15.73	0.296	15.79	0.262	16.27	0.110	13.75	0.188
Na_2O	5.01	0.162	2.59	0.181	3.03	0.255	2.89	0.174	2.39	0.081	3.79	0.216
K_2O	0.32	0.060	0.11	0.025	0.18	0.056	0.21	0.031	0.14	0.016	0.23	0.118
Total	101.00		100.63	0.501	99.56	0.391	99.87	0.607	100.59	0.491	101.46	0.278
An	55.90	1.302	76.40	1.809	73.48	2.071	74.23	1.300	78.34	0.587	65.87	0.951
Ab	42.34	1.570	22.97	1.748	25.55	1.899	24.61	1.456	20.85	0.631	32.84	1.601
Or	1.76	0.320	0.63	1.158	0.97	0.310	1.16	0.187	0.81	0.095	1.30	0.687

Component	KV-465		KV-466		KV-475		KV-477		KV-478		KV-486	
	1458		1477		1665		1707		1427		1910	
	ave. (6)	conf. lev.	ave. (6)	conf. lev.	ave. (6)	conf. lev.	ave. (6)	conf. lev.	ave. (6)	conf. lev.	ave. (2)	conf. lev.
SiO_2	51.93	0.278	51.73	0.540	52.79	0.276	53.60	0.475	53.76	0.623	55.67	0.364
Al_2O_3	30.78	0.076	30.37	0.334	29.92	0.396	29.18	0.283	29.42	0.461	28.80	0.036
FeO	0.44	0.028	0.46	0.041	0.55	0.066	0.56	0.035	0.48	0.074	0.23	0.036
CaO	13.06	0.237	13.56	0.420	12.82	0.237	12.26	0.202	12.32	0.323	11.07	0.075
Na_2O	4.59	0.145	4.44	0.279	4.75	0.076	4.98	0.071	4.78	0.231	5.76	0.154
K_2O	0.18	0.036	0.20	0.058	0.28	0.095	0.26	0.047	0.36	0.078	0.30	0.113
Total	100.92	0.269	100.65	0.204	101.01	0.479	100.85	0.653	101.12	0.587	101.84	0.353
An	60.65	1.016	62.64	1.909	59.44	1.232	56.79	0.597	57.60	1.529	50.65	0.507
Ab	38.50	1.024	36.26	1.937	39.04	1.483	41.77	0.710	40.40	1.727	47.71	1.121
Or	0.80	0.265	1.10	0.315	1.52	0.529	1.44	0.245	2.00	0.432	1.64	0.623

* Sample no.

** Position in the vertical section (m).

*** Average of the number of analyses specified in parentheses; conf. lev. is the confidence level.

mineral and in the vertical section of the intrusion as a whole. Microprobe profiles across plagioclase grains reveal their zoning. The cores of the grains are usually more calcic (by 7–10 mol %) than the margins.

The cores of the crystals are the most interesting, because they were in equilibrium with the melt from which they crystallized. By comparing the compositions of the most calcic parts of plagioclase grains in the vertical section of the intrusion, we have determined that the average composition of the plagioclase corresponds to $An_{75–77}$ and practically does not vary (note that these data pertain only to the two- and three-mineral assemblages, and we did not study plagioclase in the bronzite assemblages). However, in the part of the

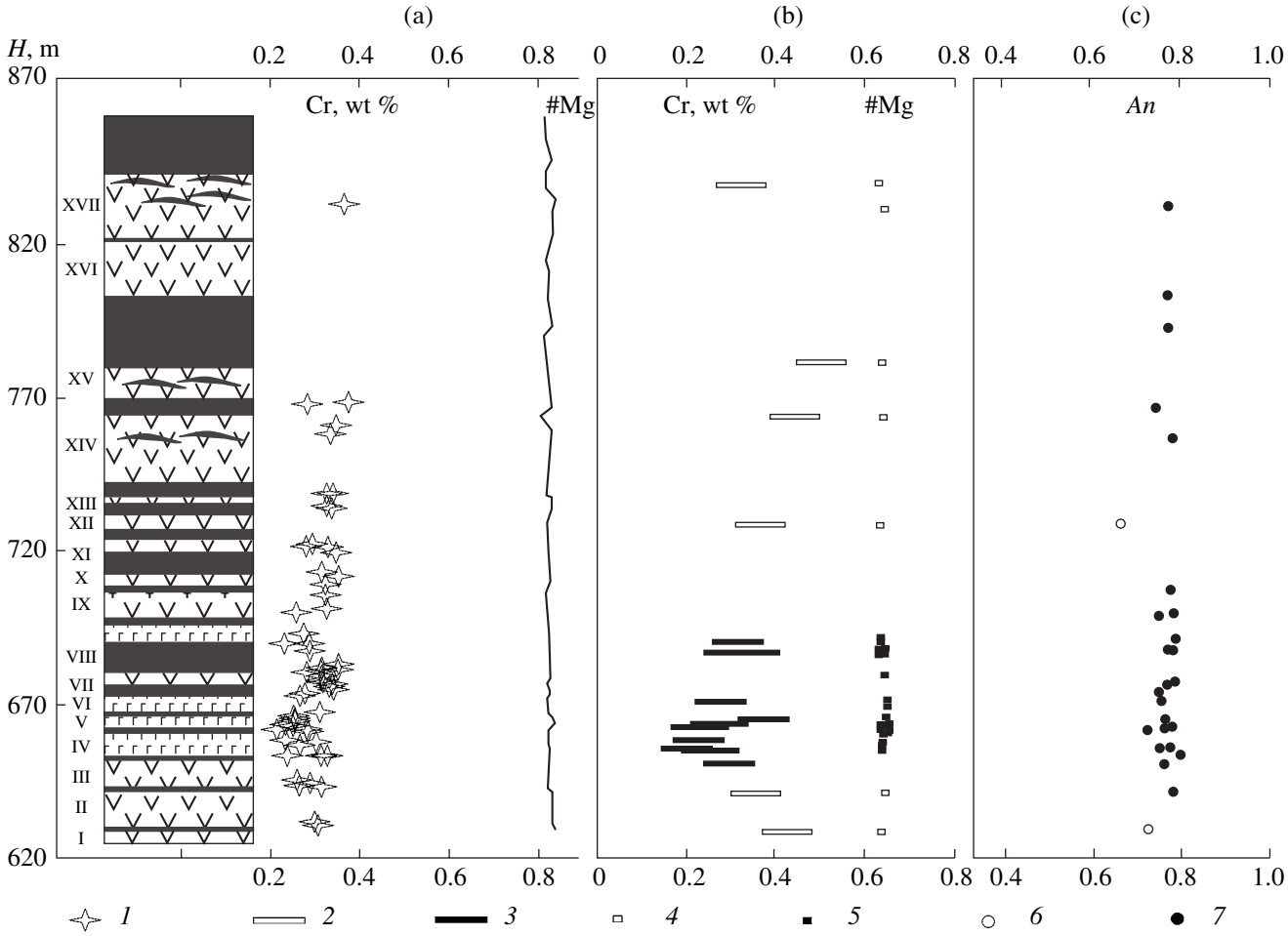

Fig. 8. Composition of minerals from the rhythmic intercalation subzone: (a) orthopyroxene; (b) clinopyroxene; (c) plagioclase. (*1*) Cr concentration, wt % (here and below, the horizontal size of a symbol is proportional to the confidence level); (*2*) Cr concentrations in intercumulus crystals; (*3*) Cr concentrations in cumulus crystals; (*4*) #Mg of intercumulus crystals; (*5*) #Mg of cumulus crystals; (*6*) intercumulus plagioclase; (7) cumulus plagioclase.

vertical section where augite appears, the cores of plagioclase grains are less calcic: up to $An_{72–75}$ (Fig. 8c). This composition of plagioclase is typical of the lower part of the Gabbro-Norite Zone (Fig. 6).

The zoning preserved in plagioclase grains reflects the evolution of the residual melt from which the plagioclase grains continued to grow. This zoning calls for more detailed consideration and analysis.

DISCUSSION AND CONCLUSIONS

The following tendencies were revealed by studying the composition of rock-forming minerals of the Kivakka intrusion.

(1) The composition of the rock-forming minerals notably vary in the vertical section of the intrusion. The #Mg of the olivine, orthopyroxene, and clinopyroxene systematically decrease up the vertical section of the intrusion, and the plagioclase simultaneously becomes less calcic.

(2) The major-component compositions of the rock-forming minerals in the Subzone of Intercalating Bronzitites and Norites remains practically unchanging over at least 250 m of the vertical section.

(3) The most contrasting variations in the Cr contents occur in the clinopyroxene. The Cr concentrations in the cumulus clinopyroxene from the central parts of gabbro-norite layers are statistically significantly lower than those in the intercumulus clinopyroxene and correspond to the Cr concentrations in augite from the lower part of the Gabbro-Norite Zone (500 m higher in the vertical section).

Our data on the compositions of minerals in the vertical section of the Kivakka layered intrusion suggest that the compositional evolution of these minerals was consistent with their theoretical crystallization sequence and the subsequent accumulation in the magmatic chamber from bottom to top. Our data on the variations in the mineral compositions are in good agreement with the evolution of the mineralogy of the

Table 3. Composition of low-Ca orthopyroxene in the vertical section of the Kivakka intrusion

Mineral assemblage	bpa*		b		b		b		b		b	
Component	rt05-2**		rt06-1		rt06-3		rt06-31		rt06-32		rt06-33	
	657.3***		660.6		660.6		661.0		661.3		661.7	
	ave. (5)****	conf. lev.	ave. (5)	conf. lev.	ave. (15)	conf. lev.	ave. (10)	conf. lev.	ave. (10)	conf. lev.	ave. (10)	conf. lev.
SiO_2	55.53	0.212	55.63	0.342	55.35	0.216	55.31	0.251	55.32	0.130	55.22	0.203
TiO_2	0.13	0.015	0.11	0.028	0.13	0.012	0.14	0.015	0.15	0.034	0.14	0.019
Al_2O_3	2.19	0.283	1.75	0.081	1.83	0.071	1.82	0.077	1.77	0.099	1.84	0.101
FeO	11.21	0.238	11.38	0.042	11.13	0.186	11.19	0.307	11.27	0.348	11.37	0.320
MnO	0.24	0.009	0.24	0.033	0.23	0.017	0.26	0.028	0.26	0.019	0.22	0.030
MgO	28.94	0.242	29.01	0.334	28.56	0.190	28.45	0.358	28.85	0.450	28.44	0.359
CaO	1.70	0.769	1.95	0.707	2.48	0.327	2.57	0.839	1.70	0.614	2.11	0.647
Na_2O	0.03	0.016	0.04	0.026	0.06	0.010	0.05	0.027	0.04	0.024	0.04	0.014
Cr_2O_3	0.33	0.048	0.34	0.086	0.36	0.039	0.40	0.031	0.31	0.034	0.36	0.025
Total	100.30	0.442	100.46	0.388	100.13	0.268	100.18	0.202	99.66	0.195	99.73	0.093
En	79.11	1.131	78.57	1.192	77.78	0.480	77.49	1.185	78.94	1.065	78.00	0.850
Fs	17.57	0.540	17.65	0.183	17.37	0.309	17.49	0.549	17.70	0.545	17.84	0.540
Wo	3.31	1.433	3.78	1.356	4.85	0.630	5.02	1.621	3.36	1.217	4.16	1.272
#Mg	0.82	0.004	0.82	0.001	0.82	0.003	0.82	0.003	0.82	0.005	0.82	0.004

Mineral assemblage	b		b		b		bpa		bpa		bpa	
Component	rt06-34		rt06-35		rt06-4		rt06-5		rt06-6		rt06-7	
	662.0		662.3		662.4		662.5		664.0		664.4	
	ave. (10)	conf. lev.	ave. (10)	conf. lev.	ave. (15)	conf. lev.	ave. (5)	conf. lev.	ave. (5)	conf. lev.	ave. (5)	conf. lev.
SiO_2	55.17	0.140	55.23	0.165	55.34	0.179	55.16	0.390	55.46	0.420	55.31	0.186
TiO_2	0.15	0.026	0.17	0.036	0.13	0.018	0.12	0.019	0.14	0.030	0.16	0.025
Al_2O_3	1.76	0.098	1.73	0.058	1.92	0.116	1.97	0.191	1.75	0.131	1.74	0.215
FeO	11.36	0.426	11.32	0.209	11.31	0.340	10.80	0.510	10.70	0.122	10.76	0.229
MnO	0.25	0.028	0.24	0.032	0.23	0.017	0.22	0.010	0.21	0.047	0.21	0.036
MgO	28.62	0.387	28.40	0.289	28.46	0.317	29.29	0.519	29.57	0.496	29.61	0.486
CaO	2.02	0.758	2.12	0.646	2.24	0.596	1.80	0.590	1.82	0.510	1.66	0.523
Na_2O	0.05	0.029	0.05	0.014	0.04	0.015	0.03	0.009	0.02	0.020	0.02	0.014
Cr_2O_3	0.36	0.052	0.38	0.043	0.39	0.041	0.34	0.067	0.37	0.068	0.27	0.090
Total	99.74	0.137	99.63	0.208	100.06	0.237	99.73	0.344	100.03	0.364	99.72	0.212
En	78.22	0.992	78.00	0.962	77.88	0.843	79.66	1.008	79.92	0.965	80.13	1.137
Fs	17.80	0.657	17.81	0.412	17.72	0.526	16.81	0.709	16.54	0.117	16.65	0.402
Wo	3.98	1.492	4.19	1.256	4.40	1.164	3.53	1.178	3.54	0.998	3.23	1.021
#Mg	0.82	0.005	0.82	0.003	0.82	0.004	0.83	0.007	0.83	0.002	0.83	0.005

Table 3. (Contd.)

Mineral assemblage	bpa		b		bp		b		b		b	
Component	rt06-2		rt07-1		rt07-2		rt08-1		rt08-3		rt08-4	
	666.7		667.2		672.9		673.9		674.9		675.7	
	ave. (4)	conf. lev.	ave. (5)	conf. lev.	ave. (5)	conf. lev.	ave. (5)	conf. lev.	ave. (5)	conf. lev.	ave. (5)	conf. lev.
SiO_2	55.63	0.289	55.68	0.322	55.52	0.115	55.55	0.191	54.89	0.243	54.94	0.118
TiO_2	0.11	0.015	0.11	0.028	0.14	0.013	0.17	0.048	0.11	0.020	0.10	0.032
Al_2O_3	1.77	0.111	1.80	0.040	1.70	0.218	1.79	0.047	1.82	0.140	1.81	0.121
FeO	11.29	0.278	11.30	0.209	11.29	0.313	11.20	0.318	10.97	0.518	11.02	0.247
MnO	0.27	0.042	0.26	0.027	0.30	0.044	0.25	0.052	0.22	0.036	0.23	0.014
MgO	29.02	0.392	28.61	0.235	28.67	0.276	28.16	0.510	28.40	0.471	28.66	0.209
CaO	1.62	0.657	2.16	0.669	2.10	0.702	2.78	0.745	2.59	1.135	1.93	0.410
Na_2O	0.02	0.018	0.05	0.023	0.03	0.006	0.05	0.029	0.05	0.035	0.03	0.023
Cr_2O_3	0.28	0.087	0.36	0.020	0.25	0.067	0.40	0.033	0.46	0.079	0.44	0.067
Total	100.00	0.416	100.34	0.518	100.00	0.399	100.34	0.201	99.49	0.332	99.16	0.108
En	79.16	1.094	78.07	0.768	78.17	1.207	76.97	1.242	77.73	1.681	78.83	0.629
Fs	17.68	0.431	17.70	0.516	17.73	0.557	17.56	0.539	17.18	0.836	17.35	0.385
Wo	3.17	1.275	4.23	1.279	4.10	1.347	5.47	1.471	5.10	2.192	3.82	0.807
#Mg	0.82	0.004	0.82	0.003	0.82	0.005	0.82	0.005	0.82	0.006	0.82	0.003

Mineral assemblage	bpa		b		bp		b		b	
Component	rt08-5		rt08-6		rt08-8		rt08-2		rt09-1	
	676.9		677.0		678.2		679.6		680.73	
	ave. (5)	conf. lev.	ave. (5)	conf. lev.	ave. (5)	conf. lev.	ave. (5)	conf. lev.	ave. (5)	conf. lev.
SiO_2	55.12	0.409	54.91	0.149	55.15	0.312	54.95	0.231	55.52	0.238
TiO_2	0.12	0.018	0.13	0.017	0.12	0.027	0.13	0.024	0.13	0.028
Al_2O_3	1.89	0.200	1.86	0.048	1.87	0.072	1.79	0.177	1.68	0.078
FeO	11.22	0.343	11.10	0.256	10.90	0.200	10.67	0.323	10.95	0.191
MnO	0.21	0.016	0.24	0.036	0.20	0.013	0.24	0.044	0.24	0.027
MgO	28.49	0.194	28.83	0.225	28.77	0.233	28.45	0.888	28.85	0.386
CaO	1.91	0.438	1.77	0.383	1.90	0.458	2.48	1.173	1.94	0.462
Na_2O	0.03	0.017	0.02	0.016	0.03	0.014	0.03	0.022	0.04	0.016
Cr_2O_3	0.46	0.123	0.43	0.042	0.38	0.047	0.40	0.060	0.35	0.071
Total	99.43	0.218	99.28	0.318	99.31	0.202	99.14	0.151	99.71	0.289
En	78.56	0.755	79.08	0.670	79.11	0.721	78.24	1.928	78.99	0.717
Fs	17.68	0.454	17.44	0.378	17.13	0.278	16.84	0.462	17.19	0.355
Wo	3.77	0.856	3.48	0.753	3.76	0.899	4.93	2.372	3.82	0.911
#Mg	0.82	0.004	0.82	0.004	0.82	0.002	0.83	0.001	0.82	0.003

* Mineral assemblages: bpa—bronzite–plagioclase–augite; bp—bronzite–plagioclas;, b—bronzite.

** Sample no.

*** Position in the vertical section (m).

**** Average of the number of analyses specified in parentheses; conf. lev. is the confidence level.

Table 4. Cr concentration in orthopyroxene from the Contrasting Intercalation Subzone of the Kivakka intrusion

Sample	H, m*	Cr **, wt % (ave. of 8)	Conf. lev.	Assemblage	Sample	H, m*	Cr **, wt % (ave. of 8)	Conf. lev.	Assemblage	Sample	H, m*	Cr **, wt % (ave. of 8)	Conf. lev.	Assemblage
rt01-1	641.7	0.30	0.022	bp	rt07-2	686.6	0.26	0.019	bpa	rt10-2	715.3	0.26	0.037	bp
rt02-1	642.7	0.29	0.019	b	rt08-1	687.6	0.28	0.015	b	rt10-3	716.9	0.32	0.009	bp
rt02-1c	642.9	0.25	0.024	b	rt08-3	688.6	0.34	0.029	b	rt11-1/99	721.0	0.32	0.009	b
rt02-1v	643.1	0.37	0.014	b	rt08-4	689.4	0.33	0.037	b	rt11-2/99	725.2	0.32	0.015	bp
rt02-2	654.8	0.30	0.012	bp	rt08-5	690.6	0.34	0.016	b	rt12-1/99	728.2	0.35	0.016	b
rt03-1	655.8	0.26	0.020	b	rt08-6	690.7	0.31	0.026	bp	rt11-1/01	735.8	0.34	0.020	b
rt03-1c	656.5	0.30	0.020	b	rt08-8	691.9	0.31	0.015	bp	rt12-1/01	738.2	0.28	0.023	b
rt03-1v	656.9	0.27	0.040	b	rt08-2	693.3	0.31	0.016	bp	rt12-2	751.9	0.33	0.022	bp
rt03-2	665.7	0.24	0.022	bp	rt09-1	694.4	0.30	0.034	b	rt13-1	752.7	0.32	0.018	b
rt04-1	665.8	0.30	0.021	b	rt09-11	694.9	0.33	0.025	b	rt13-1c	752.9	0.32	0.007	b
rt04-1v	665.8	0.31	0.024	b	rt09-12	695.4	0.31	0.042	b	rt13-1v	753.0	0.29	0.015	b
rt04-2	669.9	0.26	0.021	bp	rt09-13	695.9	0.29	0.044	b	rt13-2	756.7	0.33	0.008	b
rt05-1	670.2	0.29	0.023	ba	rt09-14	696.4	0.34	0.022	b	rt14-1	756.8	0.32	0.018	b
rt05-2	670.9	0.23	0.012	bpa	rt09-15	696.9	0.29	0.035	b	rt14-2	777.9	0.33	0.039	bp
rt06-1	674.3	0.27	0.008	b	rt09-2	704.0	0.23	0.034	bpa	rt15-1	780.5	0.34	0.022	b
rt06-2	680.4	0.40	0.063	bpa	rt09-3	704.4	0.26	0.043	bpa	rt15-2	787.9	0.28	0.037	bp
rt07-1	680.9	0.30	0.085	b	rt09-5	707.7	0.29	0.035	bpa	rt16-1	788.3	0.37	0.010	b
rt07-1c	681.4	0.28	0.032	b	rt10-1c	714.7	0.31	0.016	b	rt17-2	857.3	0.36	0.053	bp
rt07-1v	681.7	0.31	0.069	b	rt10-1i	715.0	0.28	0.034	b					

* Position in the vertical section of the intrusion (m).

** Cr concentrations calculated as averages of eight analyses; mineral assemblages: bpa—bronzite–plagioclase–augite; bp—bronzite–plagioclase; ba—bronzite–augite; b—bronzite.

Kivakka Massif, which was calculated by the mathematical simulation with the COMAGMAT computer program (based on the convection–cumulus model for the evolution of magmatic melts [15, 16]). This program makes it possible to quantitatively reproduce the general tendencies in the distribution of minerals and elements in the vertical sections of layered intrusions. The composition of the model liquidus olivine occurred to be close to that of olivine contained in the rocks, which can be regarded as validating the interpretation

Table 5. Composition of high-Ca clinopyroxene in the Rhythmic Intercalation Subzone of the Kivakka intrusion

Mineral assemblage	bpa*		ba		bpa		bpa		bpa		bpa	
Component	rt04-2**		rt05-1		rt05-2		rt05-3		rt06-6		rt06-7	
	656.2***		656.5		657.2		660.5		664.0		664.4	
	ave. (5)****	conf. lev.	ave. (5)	conf. lev.	ave. (4)	conf. lev.	ave. (4)	conf. lev.	ave. (2)	conf. lev.	ave. (3)	conf. lev.
SiO_2	52.61	0.273	53.18	0.493	52.82	1.086	52.99	0.123	53.28	0.265	53.04	0.388
TiO_2	0.22	0.010	0.27	0.017	0.30	0.028	0.22	0.031	0.21	0.004	0.45	0.014
Al_2O_3	2.78	0.083	2.77	0.054	2.81	0.200	2.97	0.084	2.96	0.113	2.59	0.073
FeO	6.15	0.834	6.56	0.695	6.36	1.224	6.24	0.681	5.85	0.568	6.89	0.479
MnO	0.17	0.046	0.16	0.039	0.15	0.035	0.11	0.028	0.14	0.025	0.19	0.034
MgO	17.63	0.328	18.10	0.752	17.58	1.447	18.09	0.853	17.03	0.040	18.59	0.876
CaO	18.69	1.413	16.66	1.935	18.61	3.391	19.22	1.444	20.59	0.459	17.08	1.465
Na_2O	0.23	0.027	0.28	0.032	0.16	0.039	0.32	0.036	0.32	0.023	0.27	0.019
Cr_2O_3	0.65	0.054	0.67	0.060	0.64	0.057	0.64	0.036	0.62	0.001	0.61	0.035
Total	99.13	0.280	98.66	0.468	99.43	0.227	100.79	0.209	101.00	0.921	99.72	0.589
En	50.75	1.175	53.26	2.664	50.66	4.509	50.99	2.122	48.40	0.843	53.14	2.258
Fs	10.22	1.496	11.09	1.276	10.52	2.119	10.04	1.117	9.55	0.755	11.35	0.766
Wo	39.03	2.631	35.64	3.883	38.81	6.616	38.97	3.032	42.06	0.088	35.52	2.988
#Mg	0.84	0.017	0.83	0.010	0.83	0.015	0.84	0.012	0.84	0.013	0.83	0.004

Mineral assemblage	bpa		bpa		bpa		bpa		bpa		b	
Component	rt06-8		rt06-2		rt07-2		rt09-2		rt09-3		kvzh4	
	665.6		666.7		672.9		690.3		690.7		852.2	
	ave. (3)	conf. lev.	ave. (5)	conf. lev.	ave. (3)	conf. lev.	ave. (3)	conf. lev.	ave. (4)	conf. lev.	ave. (3)	conf. lev.
SiO_2	52.05	0.202	52.57	0.163	52.40	0.212	52.74	0.625	53.07	0.585	52.12	0.276
TiO_2	0.36	0.147	0.30	0.085	0.25	0.016	0.21	0.018	0.25	0.042	0.23	0.018
Al_2O_3	2.86	0.269	2.85	0.123	2.73	0.078	3.17	0.050	3.18	0.066	2.92	0.133
FeO	5.08	0.408	5.66	0.166	5.69	0.534	6.03	0.304	6.30	0.516	6.33	0.505
MnO	0.13	0.039	0.14	0.047	0.17	0.049	0.16	0.023	0.15	0.030	0.18	0.038
MgO	16.24	0.366	17.49	0.348	17.43	0.589	17.16	0.343	17.21	0.326	18.42	1.107
CaO	21.78	1.221	20.18	0.503	19.42	1.001	19.11	0.559	19.53	0.976	17.69	1.861
Na_2O	0.38	0.044	0.30	0.016	0.27	0.024	0.28	0.022	0.30	0.048	0.35	0.056
Cr_2O_3	0.68	0.085	0.83	0.286	0.70	0.052	0.83	0.084	0.72	0.072	0.74	0.079
Total	99.57	0.512	100.32	0.282	99.05	0.205	99.67	0.630	100.72	0.253	98.98	0.353
En	46.65	1.380	49.62	0.882	50.05	1.465	49.69	0.812	49.38	1.131	52.94	3.131
Fs	8.40	0.768	9.22	0.317	9.41	0.808	10.02	0.446	10.38	0.929	10.50	0.864
Wo	44.95	2.136	41.16	1.107	40.53	2.222	40.29	1.131	40.25	1.789	36.56	3.836
#Mg	0.85	0.007	0.85	0.003	0.85	0.009	0.84	0.006	0.83	0.011	0.84	0.007

* Mineral assemblages: bpa—bronzite–plagioclase–augite; ba—bronzite–augite; b—bronzite.

** Sample no.

*** Position in the vertical section (m).

**** Average of the number of analyses specified in parentheses; conf. lev. is the confidence level.

Table 6. Composition of plagioclase in the Rhythmic Intercalation Subzone of the Kivakka intrusion

Mineral assemblage	bp*		bp		bpa		bpa	
Component	rt02-2**		rt03-2		rt04-2		rt05-2	
	654.8***		665.7		669.9		670.9	
SiO_2	49.41	49.41	49.57	48.29	50.01	49.17	49.29	48.58
Al_2O_3	32.29	32.14	32.08	32.86	31.60	32.30	32.60	32.70
FeO	0.39	0.47	0.33	0.35	0.38	0.30	0.42	0.50
MgO	0.07	0.08	0.07	0.06	0.06	0.06	0.05	0.04
CaO	15.86	16.13	15.44	15.45	14.49	16.08	15.50	16.16
Na_2O	2.52	2.29	2.82	2.40	3.28	2.46	2.30	2.36
K_2O	0.16	0.17	0.18	0.15	0.25	0.16	0.14	0.17
Total	100.68	100.69	100.50	99.55	100.07	100.52	100.30	100.53
An	76.94	78.60	73.61	77.20	71.08	77.65	72.82	78.42
Mineral assemblage	bpa		bpa		bpa		bpa	
Component	rt06-5		rt06-6		rt06-7		rt06-8	
	676.2		677.7		678.1		679.3	
SiO_2	49.09	49.06	49.39	49.89	49.63	49.98	49.81	48.96
Al_2O_3	32.77	32.78	32.39	32.58	32.13	32.27	32.24	32.50
FeO	0.41	0.33	0.39	0.45	0.47	0.46	0.42	0.43
MgO	0.09	0.05	0.05	0.04	0.06	0.04	0.08	0.09
CaO	15.30	15.48	15.56	16.05	14.86	15.95	15.30	15.80
Na_2O	2.77	2.67	2.61	2.27	3.32	2.45	2.73	2.28
K_2O	0.12	0.14	0.21	0.16	0.08	0.07	0.18	0.24
Total	100.55	100.50	100.61	100.43	100.55	100.22	100.76	100.30
An	74.85	75.66	75.74	78.70	72.82	77.87	74.71	77.95
Mineral assemblage	bpa		bpa		bp		bp	
Component	rt06-2		rt07-2		rt08-6		rt08-8	
	680.4		686.6		690.7		691.9	
SiO_2	49.34	48.99	49.93	49.28	48.65	48.41	48.75	48.24
Al_2O_3	32.20	32.80	32.01	32.39	32.31	31.71	32.15	32.33
FeO	0.44	0.32	0.47	0.37	0.35	0.38	0.45	0.40
MgO	0.03	0.02	0.03	0.01	0.05	0.04	0.07	0.04
CaO	15.72	15.42	14.93	16.04	16.18	16.59	15.95	16.55
Na_2O	2.83	2.46	2.97	2.47	2.59	2.38	2.68	2.39
K_2O	0.22	0.16	0.21	0.24	0.18	0.19	0.18	0.14
Total	100.77	100.17	100.54	100.80	100.30	99.70	100.23	100.08
An	73.68	77.01	72.71	77.21	75.77	78.92	74.94	77.33
Mineral assemblage	bp		bpa		bpa		bpa	
Component	rt08-2		rt09-2		rt09-3		rt09-5	
	693.3		704.0		704.4		707.7	
SiO_2	48.90	48.65	49.60	48.72	49.15	49.54	48.87	48.60
Al_2O_3	32.45	32.43	32.32	32.58	32.58	32.47	32.42	32.53
FeO	0.42	0.37	0.33	0.38	0.49	0.50	0.53	0.36
MgO	0.08	0.03	0.04	0.06	0.08	0.09	0.07	0.06
CaO	16.27	16.67	15.66	16.24	15.29	15.50	15.85	16.48
Na_2O	2.51	2.30	2.74	2.30	2.62	2.24	2.59	2.24
K_2O	0.20	0.17	0.09	0.15	0.18	0.15	0.15	0.16
Total	100.83	100.62	100.76	100.42	100.39	100.48	100.48	100.42
An	76.19	79.51	75.63	78.92	75.65	77.28	76.66	79.64

Table 6. (Contd.)

Mineral assemblage	bp		bp		bpa		bpa	
Component	rt10-2		rt10-2		rt11-2		rt14-2	
	715.3		716.9		725.2		777.9	
SiO_2	49.49	49.03	49.10	49.75	48.25	48.34	47.90	48.59
Al_2O_3	32.79	32.53	32.51	32.39	32.06	32.07	32.94	32.93
FeO	0.31	0.42	0.47	0.37	0.52	0.42	0.40	0.39
MgO	0.14	0.09	0.09	0.05	0.06	0.03	0.02	0.06
CaO	13.68	15.89	15.68	15.61	16.15	16.31	15.68	15.60
Na_2O	2.74	2.64	2.39	2.25	2.46	2.41	2.69	2.38
K_2O	1.12	0.17	0.18	0.18	0.18	0.18	0.15	0.16
Total	100.28	100.76	100.41	100.60	99.69	99.77	99.77	100.10
An	68.49	75.58	77.70	78.30	76.38	78.40	75.85	77.86

Mineral assemblage	bp		bp		bp	
Component	rt15-2		rt16-2		rt17-2	
	787.9		816.2		857.3	
SiO_2	50.34	47.77	48.98	48.31	49.13	47.57
Al_2O_3	31.72	32.76	32.67	32.59	32.21	32.89
FeO	0.33	0.39	0.31	0.38	0.30	0.28
MgO	0.06	0.07	0.06	0.06	0.03	0.04
CaO	14.27	15.38	15.43	16.12	15.09	16.21
Na_2O	3.18	2.50	2.73	2.35	3.03	2.11
K_2O	0.35	0.23	0.28	0.24	0.09	0.19
Total	100.24	99.10	100.45	100.05	99.88	99.29
An	69.87	76.32	74.73	77.39	74.29	80.18

Note: For each sample, analyses with the maximum and minimum *An* contents are presented.

* Mineral assemblages: bpa—bronzite–plagioclase–augite; bp—bronzite–plagioclase.

** Sample no.

*** Position in the vertical section (m).

of olivinites as an inherent member of the differentiated rock series of the massif, which is dominated by intratelluric olivine phenocrysts that were contained in the parental magma. The overall evolutionary scheme of other rock-forming minerals is consistent with the concept that the rocks of the massif were formed in compliance with the mechanism of crystallization differentiation. The elevated #Mg of orthopyroxene in the ultramafic part of the massif and its gradual decrease in the ortho- and clinopyroxene of the norites and gabbronorites was interpreted as resulting from the differentiation of a single parental magma and is well reproduced in the numerical model. A notable evolution of the plagioclase composition was noted in the norites and gabbro-norites, in which plagioclase is a cumulus mineral. Thus, our data are consistent with the fractionation concept of the parental melt.

The tendencies in the variations in the compositions of minerals in the vertical section of the intrusion as a whole imply repeated variations in the compositions of minerals in the zone of contrasting intercalations, because they belong to different mineral assemblages. However, pyroxenes in this part of the vertical section are characterized by the constancy of such of their important compositional parameters as #Mg. The mathematical simulation of the evolution of the Kivakka magmatic melt with the COMAGMAT computer program indicates that the transition from the bronzite to bronzite–plagioclase cotectic is associated with variations in the compositions of rock-forming minerals of no more than 5 mol % (Fig. 9). The orthopyroxene occurs in the part of the vertical section for which a change in the cumulus mineral assemblages was suggested, and its compositional variations correspond to the simulated ones. Thus, the concentrations of major components in the mineral was proved to be uninformative.

An almost identical result was obtained for the concentrations of trace elements in the orthopyroxene. In spite of the general tendency toward a decrease in the Cr concentration in the bronzite in the interval of the vertical section with gabbro-norite layers, these varia-

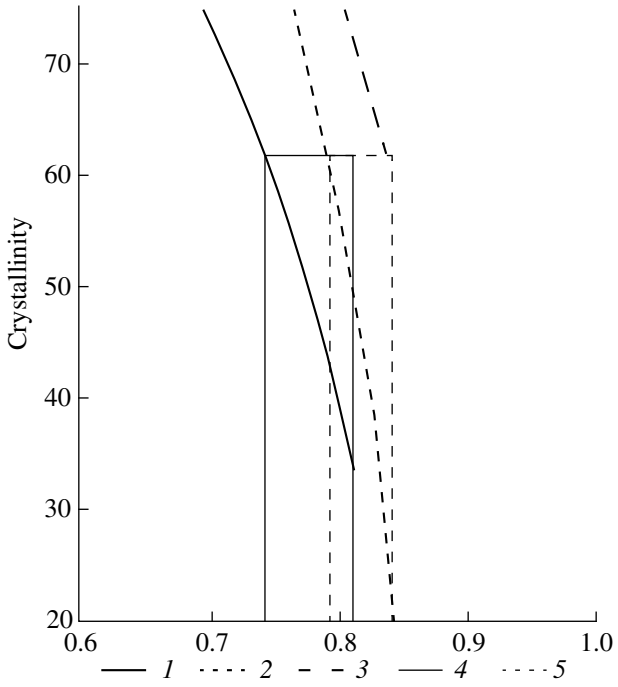

Fig. 9. Calculated changes in the compositions of minerals in the transition zone from the bronzite to bronzite–plagioclase and bronzite–plagioclase–augite cotectics. (*1*) Compositional trend of the low-Ca pyroxene; (*2*) compositional trend of the plagioclase; (*3*) compositional trend of the high-Ca pyroxene; (*4*) range of the compositional variations in the low-Ca pyroxene; (*5*) range of the compositional variations in the plagioclase.

tions remain within the confidence level and cannot be unambiguously and strictly interpreted as a decrease in the concentration of this element. Nevertheless, a decrease in the Cr concentration was detected for whole-rock samples within the interval with the three-mineral assemblage [17].

The most contrasting distribution in minerals in various layers composing rhythmic intercalations is typical of Cr in clinopyroxene. As was shown above, the concentrations of this element in the intercumulus augite of the norite is statistically significantly higher (but not lower) in the intercumulus augite of the norites than in the cumulus clinopyroxene of the gabbro-norites. If the melanocratic norites and gabbro-norites were formed simultaneously, then significant Cr amounts should have been incorporated into the cumulus clinopyroxene (with regard for the mineral–melt distribution coefficients, equal to approximately 8). In this situation, the Cr concentrations in the intercumulus augite that crystallized from the residual melt should have been lower. In fact, the relations are the opposite, and the intercumulus liquid contains more Cr than the melt from which the gabbro-norites with cumulus clinopyroxene crystallized. This is corroborated by a decrease in the Cr concentration in gabbro-norite layers [17]. These facts led us to suggest that the cumulus augite crystallized from a more fractionated magma than the residual melt from which the intercumulus clinopyroxene crystallized, because magma fractionation simultaneous with clinopyroxene crystallization should have resulted in the depletion of the melt in Cr. It should also be mentioned that the Cr concentration in the cumulus augite (as in the whole rocks) in this part of the vertical section is close to the Cr concentration in rocks 500 m higher in the vertical section, within the interval of the pervasive appearance of cumulus clinopyroxene in the Gabbro-Norite Zone.

Our results provide arguments in support of the multilayer–suspension hypothesis proposed in [9] to account for the genesis of rhythmic layering. According to this hypothesis, the material forming near the roof from a more evolved melt should be added to the matrix of the more primitive suspension corresponding to the less fractionated magma.

ACKNOWLEDGMENTS

The authors thank S.A. Vorob'ev and N.N. Pchelintseva of the Department of Geochemistry, Moscow State University, for consultations concerning the statistically accurate processing and interpretation of our data. A.A. Yaroshevskii, A.Yu. Bychkova, and A.A. Ariskin (Vernadsky Institute of Geochemistry and Analytical Chemistry, Russian Academy of Sciences) are thanked for the discussion of the results. This study was financially supported by the Russian Foundation for Basic Research (project nos. 02-05-65168, 06-05-64649), expedition projects 99-05-79051, 00-05-79089, and 01-05-79108, 02-05-79101, and the Geomodel Project of the Program "Russian Universities."

REFERENCES

1. Ya. V. Bychkova and E. V. Koptev-Dvornikov, "Types of Parental Magmas of Fennoscandian Mafic–Ultramafic Intrusions as a Classification Criterion," in *Proceedings of International Conference on Rifting, Magmatism, and Metallogeny in the Precambrian. Correlation of the Fennoscandian Geological Complexes, Petrozavodsk, Russia, 1999* (Petrozavodsk, 1999), pp. 20–21 [in Russian].
2. *Layered Intrusions*, Ed. by R. G. Cawthorn (Elsevier, Amsterdam, 1996).
3. F. J. Kruger and J. S. Marsh, "The Mineralogy, Petrology and Origin of the Merensky Cyclic Unit in the Western Bushveld Complex," Econ. Geol. **80** (4), 958–974 (1985).
4. W. P. Muerer and A. E. Boudreau, "Petrology and Mineral Composition of the Middle Banded Series of the Stillwater Complex, Montana," J. Petrol. **37**, 583–607 (1996).
5. A. H. Wilson, "The Geology of the Great Dyke, Zimbabwe: Crystallization, Layering and Cumulate Formation in the *Pl Pyroxenite of Cyclic Unit 1 of the Darwendale Subchamber,*" J. Petrol. **33**, 611–633 (1992).

6. A. H. Wilson, C. A. Lee, and R. T. Brown, "Geochemistry of the Merensky Reef, Rustenburg Section, Bushveld Complex: Controls on the Silicate Framework and Distribution of Trace Elements," Miner. Deposita **34**, 756–672.
7. E. V. Koptev-Dvornikov, B. S. Kireev, N. F. Pchelintseva, and D. M. Khvorov, "Distribution of Cumulative Mineral Assemblages, Major and Trace Elements over the Vertical Section of the Kivakka Intrusion, Olanga Group of Intrusions, Northern Karelia," Petrologiya **9**, 3–27 (2001) [Petrology **9**, 1–24 (2001)].
8. M. M. Lavrov, "Ultramafic and Layered Peridotite–Gabbro–Norite Intrusion of Precambrian of Northern Karelia," in *Nauka* (Leningrad, 1979) [in Russian].
9. Yu. V. Amelin and V. S. Semenov, "Age and Magmatic Sources of Karelian Lower Proterozoic Layered Intrusions," in *Proceedings of Conference on Isotope Dating of Endogenous Ore Formations* (Tbilisi, 1990), pp. 40–42 [in Russian].
10. A. Yu. Barkov, L. F. Gannibal, G. I. Ryungenen, and Yu. A. Balashov, "Dating of Zircons from the Kivakka Layered Massif, Northern Karelia," *Proceedings of All-Russia School-Seminar on Methods of Isotopic Geology*, (St. Petersburg, 1991), pp. 21–23 [in Russian].
11. Yu. V. Amelin and V. S. Semenov, "Nd and Sr Isotope Geochemistry of Mafic Layered Intrusions in the Eastern Baltic Shield: Implications for the Sources and Contamination of Paleoproterozoic Continental Mafic Magmas," Contrib. Miner. Petrol. 1996. **124**, pp. 255–272.
12. Ya. V. Bychkova and E. V. Koptev–Dvornikov, "Rhythmic Layering of the Kivakka Type: Geology, Petrography, Petrochemistry, and a Hypothesis for Its Formation," Petrologiya **12** (3), 281–302 (2004) [Petrology **12**, 244–264 (2004)].
13. J. D. Miller, E. M. Ripley, and Jr. Ripley, "Layered Intrusions of the Duluth Complex," Minnesota, USA. In: *Layered intrusions*. Ed. by G. Cawthorn (1996), pp. 257–302.
14. A.H. Wilson, "The great dyke of Zimbabwe," In: *Layered intrusions*. Ed. by G. Cawthorn (1996), pp. 365–402.
15. A. A. Ariskin and G. S. Barmina, *Modeling of Phase Equilibria during Crystallization of Basaltic Magmas* (MAIK "Nauka/Interperiodika", Moscow, 2000) [in Russian].
16. M. Ya. Frenkel', A. A. Yaroshevskii, A. A. Ariskin, et al., *Dynamics of Within-Chamber Differentiation of Basic Magmas* (Nauka, Moscow, 1988) [in Russian].
17. N. F. Pchelintseva and E. V. Koptev-Dvornikov, "Chromium as an Indicator of Emplacement Processes of the Kivakka Layered Intrusion," in *Proceeding of Internations (10th Al-Russian) Petrographical Conference "Petrography of 21st Century"* (Apatity, 2005), Vol. 3, pp. 232–233 [in Russian].